IEEE Photonics Journal
An IEEE Photonics Society Publication

Open Access

# Generation of Tunable Fractional Vector Curvilinear Beams With Controllable Phase Distribution

Volume 11, Number 6, December 2019

Fengyan Gu
Zhongzheng Gu
Chenliang Chang
Caojin Yuan
Shaotong Feng
Fangjian Xing
Shouping Nie

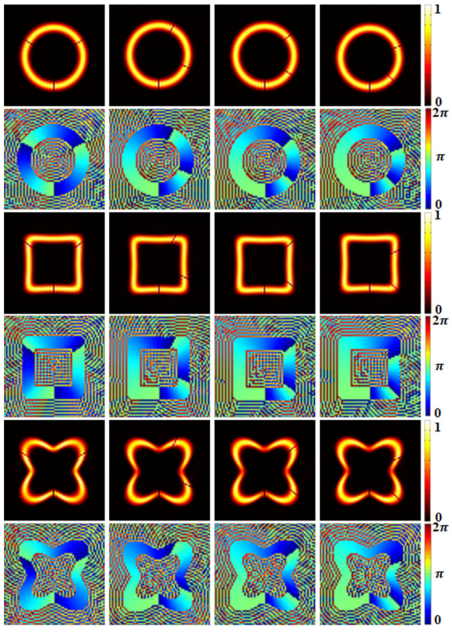


DOI: 10.1109/JPHOT.2019.2942041

# Generation of Tunable Fractional Vector Curvilinear Beams With Controllable Phase Distribution

**Fengyan Gu,[1] Zhongzheng Gu,[1] Chenliang Chang,[1] Caojin Yuan,[1,2] Shaotong Feng,[1] Fangjian Xing,[1] and Shouping Nie[1]**

[1]Key Laboratory for Opto-Electronic Technology of Jiangsu Province, Nanjing Normal University, Nanjing 210023, China
[2]Jiangsu Center for Collaborative Innovation in Geographical Information Resource Development and Application, Nanjing 210023, China

*DOI:10.1109/JPHOT.2019.2942041*


Manuscript received June 19, 2019; revised August 26, 2019; accepted September 14, 2019. Date of publication September 18, 2019; date of current version October 5, 2019. This work was supported by the National Key Research and Development Program under Grant 2017YFB0503505; National Natural Science Foundation of China (61605080, 61775097, and 61575095), and in part by the Open Foundation of Key Lab of Virtual Geographic Environment (Nanjing Normal University), Ministry of Education (2017VGE02) and the Natural Science Foundation of Jiangsu Province (Grant no. BK20190697).
Corresponding authors: Fangjian Xing; Shouping Nie (e-mail: fangjian_xing@njnu.edu.cn; nieshouping@njnu.edu.cn).

**Abstract:** An approach to generate the tunable fractional vector curvilinear beams (VCBs) was proposed. The scheme is based on the vector optical field generator (VOFG) system, where the two orthogonal polarized scalar curvilinear beams (SCBs) are generated to be the base vector components, and coaxially superposed by a Ronchi grating. We design a new phase distribution with several loops of 0 to $\pi$ in order to generate more dark gaps. The phase distribution becomes nonuniform by varying the phase variation rate and the positions of the dark gaps are changed. Using the different parameters of the curves, the fractional VCBs with different shapes are achieved. The two orthogonal polarized SCBs with the opposite topological charges are modulated to perform the beam conversion by a phase-only computer-generated hologram (CGH). Our experimental results comply with the theory and the radial opening of the dark gaps may have some applications for guiding and transporting particles.

**Index Terms:** Tunable, phase distribution, dark gaps, beam shaping.

## 1. Introduction

The vector beam (VB) plays a very important role in the long history of the optical development. As is known to all, VB has attracted a lot of attention due to its special features with spatially polarized structures, which have been used for laser processing of materials [1], [2], imaging application [3], [4], optical manipulation and optical trapping [5]. Recently, many methods of VBs generation have been proposed, and some of them designed and used the special optical elements, such as conical Brewster prism [6], single plasmonic metasurface [7], subwavelength gratings [8], [9], and interferometers [10]. Also, there are some other methods to directly generate VBs via the specially designed lasers [11], [12]. In 2016, Li *et al.* proposed the concept of the perfect vector beam (PVB) [13], which is a combination of the VB and the perfect optical vortex (POV) [14]. In 2018, Pradhan

*et al.* reported the generation of the perfect cylindrical vector beams (PCVBs) [15]. Based on the special interferometric method, the ring width and diameter are completely controlled, respectively.

Beam shaping has extensive effects on optical trapping [16], and the design of more shapes of the vortex beam can be widely used in the optical cage [17], optical regulation and acceleration of microparticles [18]. Subsequently, many ideas of applying beam shaping to scalar field have been proposed. In 2017, Kovalev *et al.* generated an elliptic perfect optical vortex (EPOV) beam [19], and Porfirev *et al.* studied the non-ring POV in 2018 [20]. Also, many works of the beam shaping using the digital micromirror device (DMD) have been reported, such as shaping the symmetric Airy beam [21] and the vortex symmetric Airy beam [22], generating the accelerating peculiar polygon beams [23] and the POV beams with large topological charges [24], and superpixel modulating the intensity and phase of the beams [25].

Due to the widespread application of VBs, the shaping of VBs becomes more important. In fact, more useful states and shapes can be provided by adjusting the degree of polarization and spatial freedom of the vector beams. In 2016, Mitchell *et al.* proposed a method to generate and switch VBs with spatially controllable intensity, phase and polarization using the DMD [26]. Afterwards, Li *et al.* applied the beam shaping to the PVB using the spatial light modulator (SLM), and achieved the elliptic perfect vector beam (EPVB) [27]. Changing from scalar field to vector field, such kind of the beam may provide more potential applications for vector optical field shaping, like complex optical trapping [28]. But it should be pointed that the beam shaping is rarely relation with the vector beams having the fractional topological charge.

Fractional optical vortex is a special vortex beam where the topological charge is a fraction [29]. The bright ring has a special and distinctive radial gap, and it will provide more additional control parameters. More investigations in the fractional optical vortex have been reported, such as the study of spiral phase about fractional vortex beams [30], [31], the orbital angular momentum, the topologically structured darkness of a fractional vortex beam [32], the "perfect" fractional vortex beams [33], and so on. Many methods generating the fractional optical vortex beams have also been proposed where different elements were used, including spiral phase plate [34], optically uniaxial crystals [35] and forked diffraction gratings [30]. Considering the unique nature, the fractional optical vortex beam may be used in optical sorting [36], guiding, transporting and trapping particles [37], the manipulation in multiple microparticle [38] and the anisotropic edge enhancement [39]. However, few reports about fractional VBs have been reported.

In this letter, the fractional optical vortex, VB and beam shaping are realized in one system, and we use a method to generate the fractional VBs along the arbitrary curves, which is called the fractional vector curvilinear beams (VCBs), and change the parameters of the curvilinear beams, in order to achieve more shapes. On this basis, we generate more dark gaps by designing fractional phase distributions, and the positions of dark gaps are changed by varying the phase variation rate. The experimental results well comply with the simulation results.

## 2. Principle of the Technique

First, we begin to shape a scalar curvilinear beam (SCB), and its intensity and phase distribution follow a prescribed 2D curve. This method was reported by using a modified technique which is a holographic beam shaping technique [40], [41]. So at the incident plane, the complex amplitude is mathematically written as

$$H(x, y) = \frac{1}{L}\int_0^T g(t)\exp\left[-\left(\frac{ik}{f}\right)|c(t)|\,(x\cos t + y\sin t)\right]dt \tag{1}$$

where $k = 2\pi/\lambda$, $\lambda$ is the light wavelength, $L$ is the length of the curve, $c(t) = [x_0(t),\ y_0(t)]$ represent the discretional 2D curve in the coordinate, and $t \in (0, T)$. The complex function $g(t)$ is calculated as

$$g(t) = \left|c'(t)\right|\exp\left[i\varphi(t)\right] \tag{2}$$

TABLE 1
Parameters of Curves

| Type of curve | $x_0(t)$ | $y_0(t)$ |
|---|---|---|
| Ring | $R_0\cos(t)$ | $R_0\sin(t)$ |
| Square | $R_0[-2\cos(t)+0.3\cos(3t)]$ | $R_0[-2\sin(t)-0.3\sin(3t)]$ |
| Polygon | $R_0\cos(t)[1-0.25\cos(ct)]$ | $R_0\sin(t)[1-0.25\cos(ct)]$ |

the parameter $c(t) = dc/dt = [x'_0(t), y'_0(t)]$, and the phase distribution function $\varphi(t)$ is expressed by

$$\varphi(t) = 2\pi l[S(t)/S(T)]^{\alpha} \tag{3}$$

where $l$ is the topological charge, $\alpha$ is a real number which is actually used for determining the phase variation rate of the curve $c(t)$. In general, when $\alpha = 1$, the phase variation is uniform, when $\alpha \neq 1$, the phase variation is nonuniform. The $|c'(t)|$ is determined by

$$|c'(t)| = \sqrt{[x'_0(t)]^2 + [y'_0(t)]^2} \tag{4}$$

It is worthwhile to note that the amplitude distribution of the field along the curve is proportional to the $|c'(t)|$, and the curve length $L$ is:

$$L = \int_0^T |c'(\tau)|\, d\tau \tag{5}$$

Consequently, the $|c'(t)|$ in Eq. (2) is a parameter to make sure the uniform distribution of intensity along the curve [40]. And the real function $S(t)$ in Eq. (3) is defined as

$$S(t) = \int_0^t |c'(\tau)|\, d\tau \tag{6}$$

it is used to control the amplitude and phase of the curve.

Then, in order to strengthen the pattern extinction phenomenon and enhance the obvious extent of the fractional radial gap, we consider to turn the above generated 2D curve beam into a curve with controllable thickness by using one of the methods which we previously reported [42]. So the complex computer-generated hologram (CGH) $E(x, y)$ is simply calculated from the summations of all the incident fields which is under the different radius of the curves, and it is mathematically written as follow:

$$E(x, y) = \sum_{i=1}^{n} A_i \cdot H_i(x, y) \tag{7}$$

where $A_i$ is a weight factor responsible of the curve, it is used to regulate the distribution of the amplitude. We choose the width to be $n = 8$ in the experiment.

In order to change the shapes of the curves, we use the method in our paper previously reported [42]. The parametric expressions of each curve $(x_0(t), y_0(t))$ are listed in Table 1, where $t \in [0, 2\pi]$, the shape of the polygon can be changed according to the value of $c$, such as trefoil ($c = 3$), quatrefoil ($c = 4$), pentagram ($c = 5$), hexagon ($c = 6$) and so on. In this paper, the case of quatrefoil ($c = 4$) is selected in the experiment, and by using different parameter expressions, we can obtain different shapes of the SCBs.

For the purpose to achieve the fractional SCBs, we change the topological charge to be half-integer. Fig. 1 shows the simulated results of the intensity patterns and the phase patterns with different curvilinear parameter expressions and topological charges $l$. As shown in Fig. 1(a1) and Fig. 1(a2), there is a dark gap on the bottom (initial position) of the intensity pattern when $l = -0.5$, but the dark gap disappears when $l = -1$. This novel and interesting phenomenon can be explained using the phase patterns. In Fig. 1(b2), when $l = -1$, the whole phase is completely and uniformly

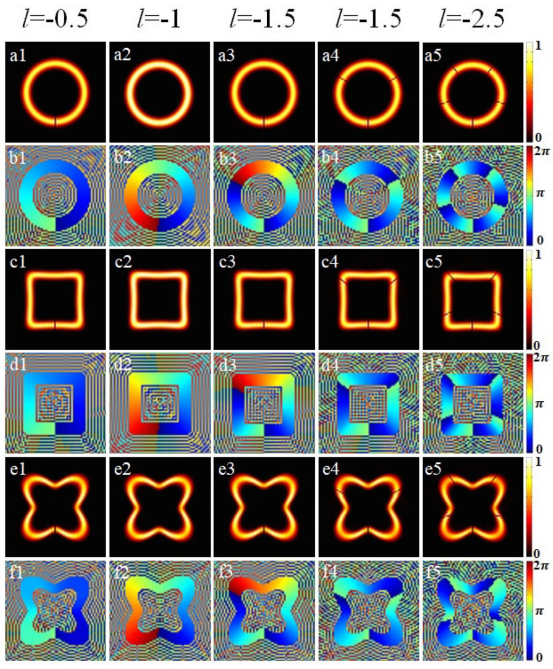


Fig. 1. The simulated results of intensity patterns and phase patterns of SCBs with different curvilinear parameter expressions and topological charges *l*.

distributed, and it increases azimuthally from 0 to $2\pi$ in a counterclockwise direction (it will increase azimuthally clockwise from 0 to $2\pi$ when $l = +1$). While $l = -0.5$, refering to Fig. 1(b1), the phase just increases from 0 to $\pi$. It should be pointed that there is no phase discontinuity when $l$ is an integer, correspondingly, the intensity patterns are complete which means no dark gap appears. A phase difference ($\pi$) on the bottom when $l = -0.5$ results to the phase discontinuity and a dark gap is showed.

Now we apply this interesting theory to the cases of higher order fractional topological charges. Fig. 1(b3) and (b4) show two different phase distributions of $l = -1.5$ at the same time. The Fig. 1(b3) is the case of normal phase pattern, which completely produces an azimuthal phase variation of $3\pi$. The phase from 0 to $2\pi$ represents the integer part, and the phase from 0 to $\pi$ indicates the fraction part. There is one phase discontinuity with the value of $\pi$ and a dark gap is located at the bottom. Instead of the case of normal phase pattern, we design a new mode of the phase [43], namely, the phase distribution is divided into three parts of 0 to $\pi$, and it produces the same azimuthal phase variation of $3\pi$. As shown in Fig. 1(b4), we change the phase distribution in normal mode. When the value of the integer part between $\pi$ and $2\pi$ minus $\pi$ is performed, the phase of the integer part is consist of two same parts (0 to $\pi$). Combining with the phase of the original fraction part, there are three phase distributions from 0 to $\pi$. The important thing is that the total phase distribution of the $3\pi$ is unchanged, which means that the topological charge still equals to 1.5. By using a conditional function to replace the original phase distribution function $\varphi(t)$ above, several phase distributions from 0 to $\pi$ can be realized. The conditional function $\varphi_2(t)$ is expressed as

$$\varphi_2(t) = \begin{cases} \varphi(t), & \text{if} \quad (m-1)\,2\pi \le \varphi(t) \le (2m-1)\,\pi, \quad m \ge 1,\, m \in \mathrm{Z} \\ \varphi(t) - (2m-1)\,\pi, & \text{if} \quad (2m-1)\pi \le \varphi(t) \le 2m\pi, \quad m \ge 1,\, m \in \mathrm{Z} \end{cases} \tag{8}$$

Where $m$ represents a complete set of integers from 1 to the integer part of the $l$, Z represents the positive integer. During one phase period from 0 to $2\pi$, the part of $\pi$ to $2\pi$ will be subtracted by $\pi$, and two phase distributions from 0 to $\pi$ appear. For example, when $l = 1.5$, $m = 1$; when $l = 2.5$, $m = \{1, 2\}$; and when $l = 5.5$, $m = \{1, 2, 3, 4, 5\}$. Based on the method, when $l = 1.5$, there are

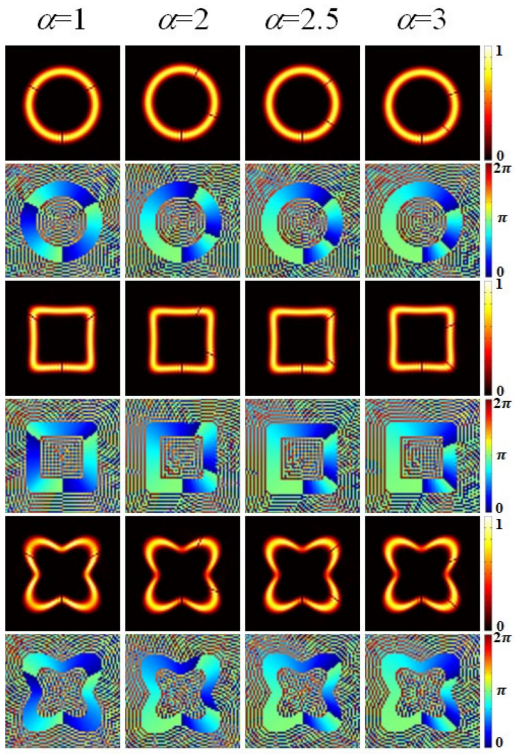


Fig. 2. The simulated results of the distinctive intensity patterns and controlled phase variations of tunable fractional SCBs with topological charge $l = -1.5$ and different parameter $\alpha$.

three dark gaps in the intensity pattern which are located at three positions with the same azimuth interval of 120°. The essential reason of the formation of these dark gaps is the discontinuity of the phase. Using this phase distribution theory, more dark gaps in the different situations are realized. We further simulated the case of $l = -2.5$, which is shown in the last column of Fig. 1. The simulation has five dark gaps, which is satisfied with our previous theory.

It is worthy mentioned that the simulation results above are carried out in the case of $\alpha = 1$, and all of the phase variations are uniformly distributed. No matter what the topological charge is and how many dark gaps there are, they are always evenly distributed by a degree of azimuth, like $l = \pm 1.5$, the dark gaps are located at each position of 120°. Now we change this situation through the parameter $\alpha$, and Fig. 2 shows the simulation results of the distinctive intensity patterns and controlled phase variations with topological charge $l = -1.5$ and different parameters $\alpha$. The results of the simulation show that the phase variation rate has been changed, and the positions of the dark gaps on the intensity patterns are also moved. It broadens the theory of the uniform distribution of the azimuth, and the uneven distribution of the dark gaps is displayed.

In the experiment, we choose the vector optical field generator (VOFG) system [44], [45]. First, we use the Eq. (1), Eq. (7) and Eq. (8), and give the opposite topological charges to calculate the complex amplitude fields of $E_L(x, y)$ and $E_R(x, y)$, which are used to generate the two base scalar beams of the fractional VCBs. Then we treat the two complex amplitude fields as two orthogonal polarized optical channels, and two phase shifting factors of $\exp(i2\pi x \sin\phi_x/\lambda)$ and $\exp(i2\pi y \sin\phi_y/\lambda)$ are imposed to each direction of the channels. Using two quarter-wave plates (QWPs), the pair of base scalar beams is transformed into the mutually orthonormal circular polarization states. Consequently, the total complex CGH which are used to generate the fractional VCBs at the incident plane is mathematically calculated as

$$E_{total}(x, y) = E_L(x, y) \cdot \exp(i2\pi x \sin\phi_x/\lambda) + E_R(x, y) \cdot \exp(i2\pi y \sin\phi_y/\lambda) \quad (9)$$

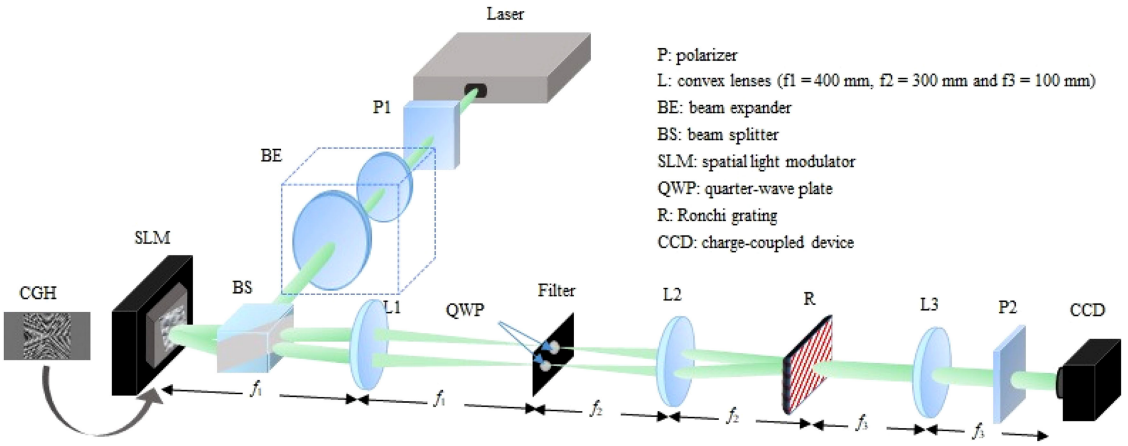


Fig. 3. Schematic representation of the experiment setup for generating fractional VCBs.

At last, we use the "double-phase" method [46], [47] to encode this complex value $E_{total}(x, y)$ into a phase-only CGH which is imprinted on a SLM (Holoeye Leto, 6.4 $\mu$m pixel pitch, 1920 $\times$ 1080 resolution).

## 3. Experimental Setup

The experiment setup of the VOFG system is shown in Fig. 3. A laser beam with a wavelength of 532 nm launched from a solid-state laser is collimated and expanded through a beam expander which is consist of two lenses. Then the beam arrives at the SLM plane, and the diffracted beams which are generated from the reflective SLM pass through the 4*f* optical filtering system, and under the influence of the two phase shifting factors which are mentioned above, the diffracted beams are spatially filtered towards horizontal (*x*-) and vertical (*y*-) direction, respectively. Two quarter-wave plates (QWPs) are immediately behind the filtering plane, to realize the function of polarization transformation of the separated beams which are converted into left and right circular polarization components. Ronchi grating is also placed at the end of the 4*f* system to achieve the coaxial superposition of this two divided base vector beams, and the last lens of L3 ($f = 100$ mm) is used to make this pair of base beams spread into the focal plane through the Fourier transformation (FT). At last, the experimental intensity patterns of the fractional VCBs are recorded by using the charge coupled device (CCD) camera, and the pattern extinction phenomenon appears by rotating the analyzer (P2).

## 4. Results and Discussion

The fractional VCBs are generated by our method, as illustrated in Figs. 4, 5, and 6. The phase distribution is divided into several parts of 0 to $\pi$. The experimental results are consistent with the expectations of the simulation. The difference of the extinction phenomenon between the polarizers (marked with red dashed circles) and fractional order (marked with blue dashed circles) is clear. Unlike the conventional topological charge of integer, the polarization state is changed in a half of phase period. While the topological charge is 0.5, the polarization state was rotated by 180 when it returns to the initial position. So the polarization state does not show the radial polarization state which is shown in the case of $l = 1$, and the polarization state is uncertainty at the initial position [44], where a dark gaps can be observed without analyzers. In the case of $l = 1.5$, the polarization state shown is equivalent to three repetition of $l = 0.5$. The dark gap occurs at the discontinuity of the phase, which means that there is an uncertain polarization state. More positions of the phase

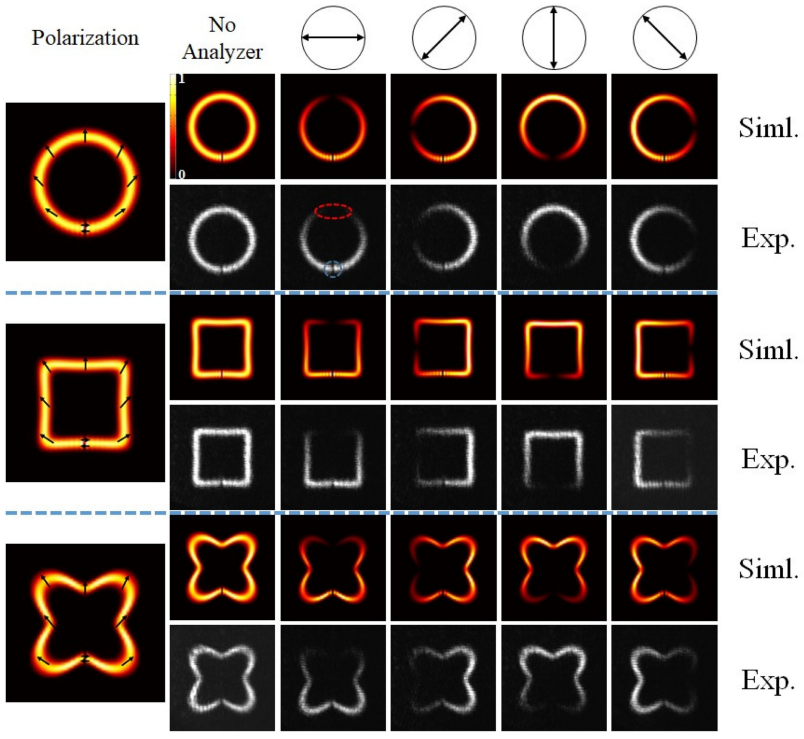


Fig. 4. Simulated and experimental results of generating fractional VCBs with topological charge $l = \pm 0.5$.

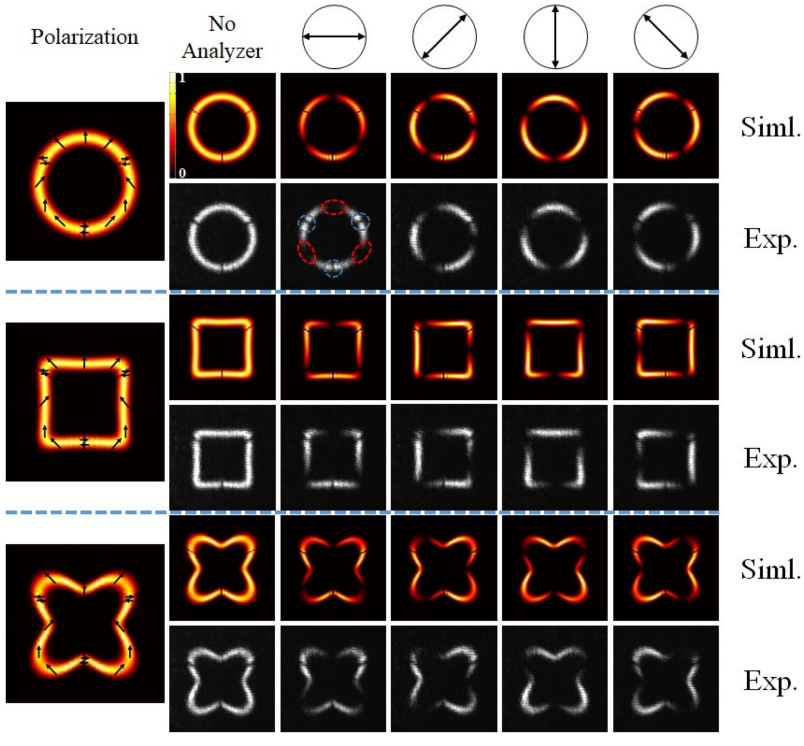


Fig. 5. Simulated and experimental results of generating fractional VCBs with topological charge $l = \pm 1.5$.

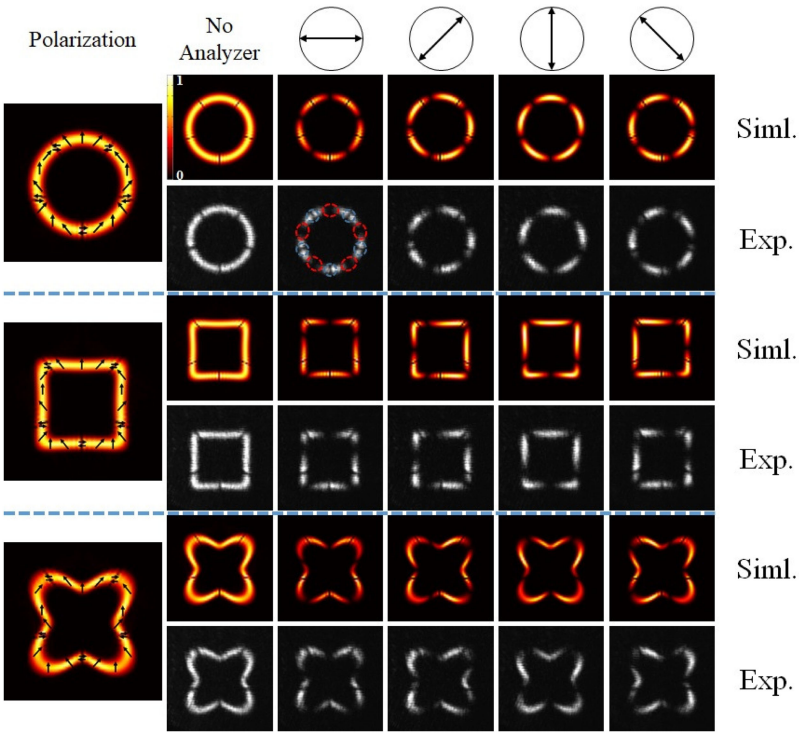


Fig. 6. Simulated and experimental results of generating fractional VCBs with topological charge $l = \pm 2.5$.

discontinuity, and more dark gaps. Using our method, when the fractional topological charge is increased, more dark gaps can be realized.

The results of the tunable fractional VCBs with controllable phase variations by changing the parameter $\alpha$ are shown in Fig. 7, we select the shape of the quatrefoil for experimental verification and choose to change the different parameters $\alpha$ with the topological charge of $l = 1.5$. Both the dark gaps caused by the fractional order (marked with blue dashed circles) and the extinction phenomenon caused by polarizers (marked with red dashed circles) have changed, the experimental results are in agreement with the simulation results. An interesting phenomenon is that the extinction region will become with the increasing of $\alpha$ when the fast axis direction of the polarizer is at 90°. The reason is that the delay of polarization gradient is caused by the retardance of the phase variation in the lower left corner.

It should be highly noted that compared with the traditional cylindrical vector beams (CVBs), the polarization structure of the fractional VCBs is asymmetric. The CVBs can be geometrically represented by the higher-order Poincaré sphere [48], and its polarization structure is rotational symmetric. When the rotational symmetry of the CVB is broken, the intrinsic vortex phases carried by the two spin components of the VB, is no longer continuous in the azimuthal direction, and leads to the spin accumulation occurring at the edge of the beam [49]. Due to the inherent nature of the phase and independency of light-matter interaction, the observed photonic spin Hall effect (SHE) is intrinsic [50]. Based on the above theory, for the fractional VCBs we proposed, due to the discontinuity of the phase, the rotational symmetry of the intensity is also broken, and it can be considered that a spin-dependent splitting (SDS), or the intrinsic photonic SHE, should present during the process of propagation. Depending on the analysis, the polarization structure of the vector polarization could not keep the initial shape during the propagation. In this regard, it may reveal some new ideas for the generation and manipulation of spin-polarized photons.

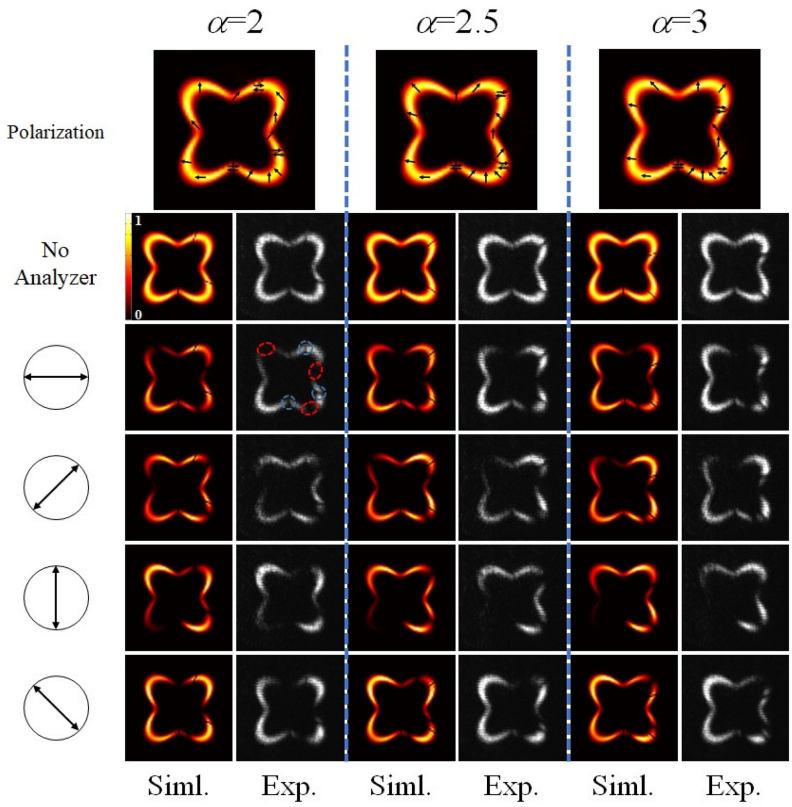


Fig. 7. Simulated and experimental results of generating the tunable fractional VCBs of the quatrefoil shape with different parameters $\alpha$ and topological charge $l = \pm 1.5$.

## 5. Conclusions

On balance, we propose a simple and feasible method which allows the generation of tunable fractional VCBs. We design the fractional phase distribution which is divided into several parts of 0 to $\pi$, and get more dark gaps. By modifying the parameter $\alpha$ in the formula, we can also adjust the phase variation rate, and control the position of the dark gaps according to the above theory of phase distribution. Then we change the parameters of curves, and obtain the tunable fractional VCBs with more shapes. In the experiment, we generate the tunable fractional VCBs by the space orthogonal superposition of two base fractional SCBs with left and right circular polarization components and opposite topological charges. Our experimental results comply with our theoretical predictions, and the radial opening of the dark gaps may be used to guide and transport particles.

## References

[1] M. Duocastella and C. B. Arnold, "Bessel and annular beams for materials processing," *Laser Photon. Rev.*, vol. 6, no. 5, pp. 607–621, 2012.
[2] R. Drevinskas, J. Zhang, M. Beresna, M. Gecevičius, A. G. Kazanskii, and Y. P. Svirko, "Laser material processing with tightly focused cylindrical vector beams," *Appl. Phys. Lett.*, vol. 108, no. 22, 2016, Art. no. 221107.
[3] Y. Kozawa and S. Sato, "Numerical analysis of resolution enhancement in laser scanning microscopy using a radially polarized beam," *Opt. Exp.*, vol. 23, no. 3, pp. 2076–2084, 2015.
[4] T. Mino, Y. Saito, and P. Verma, "Control of near-field polarizations for nanoscale molecular orientational imaging," *Appl. Phys. Lett.*, vol. 109, no. 4, 2016, Art. no. 041105.
[5] Y. Kozawa and S. Sato, "Optical trapping of micrometer-sized dielectric particles by cylindrical vector beams," *Opt. Exp.*, vol. 18, no. 10, pp. 10828–10833, 2010.

[6] Y. Kozawa and S. Sato, "Generation of a radially polarized laser beam by use of a conical Brewster prism," *Opt. Lett.*, vol. 30, no. 22, pp. 3063–3065, 2005.
[7] F. Yue, D. Wen, J. Xin, B. D. Gerardot, J. Li, and X. Chen, "Vector vortex beam generation with a single plasmonic metasurface," *ACS Photon.*, vol. 3, no. 9, pp. 1558–1563, 2016.
[8] A. Niv, G. Biener, V. Kleiner, and E. Hasman, "Manipulation of the Pancharatnam phase in vectorial vortices," *Opt. Exp.*, vol. 14, no. 10, pp. 4208–4220, 2006.
[9] Z. Bomzon, G. Biener, V. Kleiner, and E. Hasman, "Radially and azimuthally polarized beams generated by space-variant dielectric subwavelength gratings," *Opt. Lett.*, vol. 27, no. 5, pp. 285–287, 2002.
[10] S. Chen, X. Zhou, Y. Liu, X. Ling, H. Luo, and S. Wen, "Generation of arbitrary cylindrical vector beams on the higher order Poincaré sphere," *Opt. Lett.*, vol. 39, no. 18, pp. 5274–5276, 2014.
[11] C. Varin and M. Piche, "Acceleration of ultra-relativistic electrons using high-intensity TM01 laser beams," *Appl. Phys. B*, vol. 74, no. 1, pp. S83–S88, 2002.
[12] J. L. Li, K. Ueda, M. Musha, A. Shirakawa, and Z. M. Zhang, "Converging-axicon-based radially polarized ytterbium fiber laser and evidence on the mode profile inside the gain fiber," *Opt. Lett.*, vol. 32, no. 11, pp. 1360–1362, 2007.
[13] P. Li *et al.*, "Generation of perfect vectorial vortex beams," *Opt. Lett.*, vol. 41, no. 10, pp. 2205–2208, 2016.
[14] A. S. Ostrovsky, C. Rickenstorff-Parrao, and V. Arrizón, "Generation of the "perfect" optical vortex using a liquid-crystal spatial light modulator," *Opt. Lett.*, vol. 38, no. 4, pp. 534–536, 2013.
[15] P. Pradhan, M. Sharma, and B. Ung, "Generation of perfect cylindrical vector beams with complete control over the ring width and ring diameter," *IEEE Photon. J.*, vol. 10, no. 1, Feb. 2018, Art. no. 6500310.
[16] M. Woerdemann, C. Alpmann, M. Esseling, and C. Denz, "Advanced optical trapping by complex beam shaping," *Laser Photon. Rev.*, vol. 7, no. 6, pp. 839–854, 2013.
[17] Y. Chen and Y. Cai, "Generation of a controllable optical cage by focusing a Laguerre–Gaussian correlated Schell-model beam," *Opt. Lett.*, vol. 39, no. 9, pp. 2549–2552, 2014.
[18] A. Kovalev, V. Kotlyar, and A. Porfirev, "Optical trapping and moving of microparticles by using asymmetrical Laguerre–Gaussian beams," *Opt. Lett.*, vol. 41, no. 11, pp. 2426–2429, 2016.
[19] A. Kovalev, V. Kotlyar, and A. Porfirev, "A highly efficient element for generating elliptic perfect optical vortices," *Appl. Phys. Lett.*, vol. 110, no. 26, 2017, Art. no. 261102.
[20] A. Porfirev and A. Kuchmizhak, "Non-ring perfect optical vortices with p-th order symmetry generated using composite diffractive optical elements," *Appl. Phys. Lett.*, vol. 113, no. 17, 2018, Art. no. 171105.
[21] Z.-X. Fang, Y.-X. Ren, L. Gong, P. Vaveliuk, Y. Chen, and R.-D. Lu, "Shaping symmetric airy beam through binary amplitude modulation for ultralong needle focus," *J. Appl. Phys.*, vol. 118, no. 20, 2015, Art. no. 203102.
[22] Z.-X. Fang *et al.*, "Interplay between topological phase and selfacceleration in a vortex symmetric airy beam," *Opt. Exp.*, vol. 26, no. 6, pp. 7324–7335, 2018.
[23] Z.-X. Fang, H.-Z. Zhao, Y. Chen, R.-D. Lu, L.-Q. He, and P. Wang, "Accelerating polygon beam with peculiar features," *Sci. Rep.*, vol. 8, 2018, Art. no. 8593.
[24] Y. Chen, Z.-X. Fang, Y.-X. Ren, L. Gong, and R.-D. Lu, "Generation and characterization of a perfect vortex beam with a large topological charge through a digital micromirror device," *Appl. Opt.*, vol. 54, no. 27, pp. 8030–8035, 2015.
[25] S. A. Goorden, J. Bertolotti, and A. P. Mosk, "Superpixel-based spatial amplitude and phase modulation using a digital micromirror device," *Opt. Exp.,* vol. 22, no. 15, pp. 17999–18009, 2014.
[26] K. J. Mitchell, S. Turtaev, M. J. Padgett, T. Čižmár, and D. B. Phillips, "High-speed spatial control of the intensity, phase and polarisation of vector beams using a digital micro-mirror device," *Opt. Exp.*, vol. 24, no. 25, pp. 29269–29282, 2016.
[27] D. Li, C. Chang, S. Nie, S. Feng, J. Ma, and C. Yuan, "Generation of elliptic perfect optical vortex and elliptic perfect vector beam by modulating the dynamic and geometric phase," *Appl. Phys. Lett.*, vol. 113, no. 12, 2018, Art. no. 121101.
[28] L. Li *et al.*, "High efficient generation of tunable ellipse perfect vector beams," *Photon. Res.*, vol. 6, no. 12, pp. 1116–1123, 2018.
[29] M. Berry, "Optical vortices evolving from helicoidal integer and fractional phase steps," *J. Opt. A*, vol. 6, no. 2, pp. 259–268, 2004.
[30] S. Tao, W. Lee, and X. Yuan, "Dynamic optical manipulation with a higher-order fractional Bessel beam generated from a spatial light modulator," *Opt. Lett.*, vol. 28, no. 20, pp. 1867–1869, 2003.
[31] S. Tao, W. Lee, and X. Yuan, "Experimental study of holographic generation of fractional Bessel beams," *Appl. Opt.*, vol. 43, no. 1, pp. 122–126, 2004.
[32] S. N. Alperin and M. E. Siemens, "Angular momentum of topologically structured darkness," *Phys. Rev. Lett.*, vol. 119, no. 20, 2017, Art. no. 203902.
[33] G. Tkachenko, M. Z. Chen, K. Dholakia, and M. Mazilu, "Is it possible to create a perfect fractional vortex beam?" *Optica*, vol. 4, no. 3, pp. 330–333, 2017.
[34] Y. Fang, Q. Lu, X. Wang, W. Zhang, and L. Chen, "Fractional-topological-charge-induced vortex birth and splitting of light fields on the submicron scale," *Phys. Rev. A*, vol. 95, no. 2, 2017, Art. no. 023821.
[35] Y. Vasylkiv, I. Skab, and R. Vlokh, "Crossover regime of optical vortices generation via electro-optic nonlinearity: The problem of optical vortices with the fractional charge generated by crystals," *J. Opt. Soc. Amer. A*, vol. 31, no. 9, pp. 1936–1945, 2014.
[36] C. S. Guo, Y. N. Yu, and Z. Hong, "Optical sorting using an array of optical vortices with fractional topological charge," *Opt. Commun.*, vol. 283, no. 9, pp. 1889–1893, 2010.
[37] S. H. Tao, X. C. Yuan, J. Lin, X. Peng, and H. B. Niu, "Fractional optical vortex beam induced rotation of particles," *Opt. Exp.*, vol. 13, no. 20, pp. 7726–7731, 2005.
[38] I. V. Basistiy, V. A. Pas'ko, V. V. Slyusar, M. S. Soskin, and M. V. Vasnetsov, "Synthesis and analysis of optical vortices with fractional topological charges," *J. Opt. A*, vol. 6, no. 5, pp. S166–S169, 2004.
[39] G. Situ, G. Pedrini, and W. Osten, "Spiral phase filtering and orientation-selective edge detection/enhancement," *J. Opt. Soc. Amer. A*, vol. 26, no. 8, pp. 1788–1797, 2009.

[40] J. A. Rodrigo and T. Alieva, "Polymorphic beams and nature inspired circuits for optical current," *Sci. Rep.*, vol. 6, 2016, Art. no. 35341.
[41] J. A. Rodrigo and T. Alieva, "Vector polymorphic beam," *Sci. Rep.*, vol. 8, 2018, Art. no. 7698.
[42] L. Li *et al.*, "Generation of optical vortex array along arbitrary curvilinear arrangement," *Opt. Exp.*, vol. 26, no. 8, pp. 9798–9812, 2018.
[43] I. Moreno, M. Sanchez-Lopez, K. Badham, J. Davis, and D. Cottrell, "Generation of integer and fractional vector beams with q-plates encoded onto a spatial light modulator," *Opt. Lett.*, vol. 41, no. 6, pp. 1305–1308, 2016.
[44] X. Wang, J. Ding, W. Ni, C. Guo, and H. Wang, "Generation of arbitrary vector beams with a spatial light modulator and a common path interferometric arrangement," *Opt. Lett.*, vol. 32, no. 24, pp. 3549–3551, 2007.
[45] Z. Chen, T. Zeng, B. Qian, and J. Ding, "Complete shaping of optical vector beams," *Opt. Exp.*, vol. 23, no. 14, pp. 17701–17710, 2015.
[46] O. Mendoza-Yero, G. Mínguez-Vega, and J. Lancis, "Encoding complex fields by using a phase-only optical element," *Opt. Lett.*, vol. 39, no. 7, pp. 1740–1743, 2014.
[47] Y. Qi, C. Chang, and J. Xia, "Speckleless holographic display by complex modulation based on double-phase method," *Opt. Exp.*, vol. 24, no. 26, pp. 30368–30378, 2016.
[48] Y. Liu, X. Ling, X. Yi, X. Zhou, H. Luo, and S. Wen, "Realization of polarization evolution on higher-order Poincaré sphere with metasurface," *Appl. Phys. Lett.*, vol. 104, no. 19, 2014, Art. no. 191110.
[49] X. Ling *et al.*, "Realization of tunable spin-dependent splitting in intrinsic photonic spin Hall effect," *Appl. Phys. Lett.*, vol. 105, no. 15, 2014, Art. no. 151101.
[50] X. Ling *et al.*, "Recent advances in the spin Hall effect of light," *Rep. Progr. Phys.*, vol. 80, 2017, Art. no. 066401.